2011

Raman Spectroscopy of Titania (TiO$_2$) Nanotubular Water-Splitting Catalysts

F. D. Hardcastle
Arkansas Tech University, fhardcastle@atu.edu

Raman Spectroscopy of Titania (TiO₂) Nanotubular Water-Splitting Catalysts

F.D. Hardcastle

Department of Physical Sciences, Arkansas Tech University, Russellville, AR 72801
Research Affiliate of the University of Arkansas at Little Rock, Department of Applied Science, UALR Nanotechnology Center,
Little Rock, Arkansas 72204

Correspondence: fhardcastle@atu.edu

Abstract

The phase composition of nanotubular TiO_2 films was correlated with photoelectrochemical activity as a function of O_2-annealing temperature. TiO_2 nanotubes have been shown to be more efficient than polycrystalline TiO_2 for the photocatalytic splitting of water. Raman spectroscopy was used to identify and quantify the amorphous and crystalline TiO_2 phases. The amorphous TiO_2 nanotubular array was found to consist of TiO_6^{8-} octahedra having the same average structure as those present in the anatase and rutile phases of TiO_2. Results show that the anatase-to-rutile transformation on Ti metal initiates at much lower temperatures compared to polycrystalline TiO_2 and this is attributed to oxygen vacancies located at the metal/oxide interface and is likely responsible for increasing the photocurrent density.

Introduction

Titanium dioxide, TiO_2, has been one of the most widely studied photocatalytic semiconducting materials since the early 1970s when Fujishima and Honda (1972) demonstrated the splitting water into H_2 and O_2 using a simple photoelectrochemical cell and illuminating a single-crystal TiO_2 photoanode (anatase) with UV light of wavelength less than 350 nm.

TiO_2 is a promising semiconducting photoanode material for water splitting using solar radiation. In addition to its low cost and availability, TiO_2 is chemically and photochemically stable, and its band edges match the redox level of water (Burda 2003). The most important requirement of a photocatalyst is its ability to generate electron–hole pairs near the catalyst surface by harvesting a significant portion of the solar spectrum. Unfortunately, the use of TiO_2 is hindered by its large band gap which allows photoconversion of only UV radiation – the band gap must be decreased if TiO_2 is to be used for visible-light applications. Much of the research to date on TiO_2-based water-splitting catalysts has focused on narrowing the band gap by incorporating dopants into the lattice structure (Sharma 2009, Ishihara 2010). In this study, we focus on the actual phase composition of the TiO_2 which has a significant impact on its performance as a photoactive catalyst.

The two most common crystalline phases of TiO_2 suitable for photochemical applications are anatase (tetragonal) and rutile (tetragonal). Amorphous TiO_2 displays little or no photoactivity. Although rutile is more thermodynamically stable and exhibits a lower band gap than anatase (3.0 eV for rutile; 3.2 eV for anatase) (Bendavid 1999), anatase is preferred for photocatalysis. Thus, the photoactivity of the TiO_2 film should be significantly improved by taking advantage of the high surface area of anatase, present as a nanotubular array, and the lower band gap energy of rutile, and the increased efficiency of electron transport of TiO_2 nanotubes (Liu 2009).

The transformation of amorphous TiO_2 to either anatase or rutile, and the temperature at which anatase is converted to rutile, depend on many variables including the method of synthesis and the presence of foreign ions (Heald 1972) which increase the number of oxygen vacancies thereby increasing the rate of rutile formation. In this study, nanotubular TiO_2 films were characterized by Raman spectroscopy. The structural information was correlated with reported photocurrent-density measurements.

Materials and Methods

Synthesis of TiO₂ Nanotubular Arrays

The TiO_2 (titania) nanotubular films were synthesized by the UALR Nanotechnology Center, UALR (Hidetaka Ishihara, Dr. Rajesh Sharma, and Dr. Alexandru S. Biris). The films were synthesized on titanium metal foil (99.9% pure, 0.5 mm thick) using a conventional anodization process (95wt% ethylene glycol + 5wt% NH_4F; 20V). A two-electrode configuration was used for anodization. Anodization was carried out at a constant potential of 20 V using a DC voltage supply (Agilent, E3640A). The anodization

current was monitored continuously using a digital multimeter (METEX, MXD 4600 A). The anodized samples were washed with distilled water to remove the occluded ions from the anodized solutions and dried in an air-oven. The Ti foil samples were annealed in an oxygen atmosphere at 400-600 °C for 6 h in a tube furnace to convert the amorphous titania to the crystalline anatase and/or rutile forms of TiO_2.

Raman Spectroscopy

Raman spectra of all TiO_2 films were collected using a LabRam Micro-Raman Spectrometer (Horiba Jobin-Yvon HR800 UV) equipped with an optical microscope and 100x objective lens for a total magnification of 1000x. An argon-ion laser (514.5 nm) or helium-neon (632.8 nm) was used for laser excitation of the Raman signal with appropriate holographic notch filters for eliminating the laser line after excitation. The laser power at the sample ranged from 1 to 3 mW, and the 1/e laser spot size was about 2 μm at the sample. The slit width of the spectrometer was typically set at 700 μm. A holographic grating having 1800 grooves/mm was used for the collection of all Raman spectra and resulted in a spectral resolution of about 1.5 cm^{-1}. Spectral analysis and curve fitting was performed with GRAMS/AI 8.00 Spectroscopy software.

Results and Discussion

The Raman spectra for bulk TiO_2 reference compounds are presented in Figure 1. The thermodynamically stable rutile phase exhibits major peaks at 610, 446, and 242 cm^{-1} and minor peaks at 818, 707, and 319 cm^{-1}. Based on the space group D_{4h}^{14} for rutile and assumed site symmetries for the Ti and O atoms within the unit cell, group-theoretical analysis shows four Raman-active "lattice vibrations" assigned as follows: A_{1g} (610 cm^{-1}) + B_{1g} (144 cm^{-1}) + B_{2g} (827 cm^{-1}) + E_g (446 cm^{-1}) (Balachandran 1982). In the present study, we use bond length / Raman frequency / covalency correlations that have proven quite useful and accurate for many chemical systems (Hardcastle 1990, Hardcastle 1991). Recent application of this approach to the titanates (Hardcastle, work in preparation) reveals the following relationship between Ti-O bond lengths, R, and Raman frequency shifts:

$$\nu_{Ti-O} = 722e^{-1.54946(R-1.809)} \qquad (1)$$

The reported Ti-O bond lengths of *4x* 1.946 Å and *2x* 1.984 Å for rutile (Cromer 1955) are consistent with

observed Ti-O bands at 610, 571 (weak), 446, and 407 (weak) cm^{-1} which yield calculated Ti-O bond lengths of *3x* 1.92, 1.96, 2.12, and 2.18 Å. The O-O interactions, based on residual valence, are calculated to occur in the 252-394-cm^{-1} region. The broad band observed near 160-240 cm^{-1} is assigned to O-O interactions involving three- and four-coordinate oxygen. The sharp feature at 143 cm^{-1} is consistent with Ti-Ti covalent interactions (2.96 Å; 0.29 valence units).

The peaks of crystalline rutile are initially observed for an amorphous sample after annealing at 400 °C and become sharper and more intense as the annealing temperature is increased, indicating increased crystallinity of the rutile phase. An unheated Ti foil shows amorphous titania (native oxide) and exhibits broad bands near 680, 580, and 450 cm^{-1} assigned to Ti-O bonds (≈ 1.85, 1.95, and 2.11 Å); broad bands at 350 and 250 cm^{-1} are assigned to O-O interactions consistent with TiO_6^{8-} octahedra that are slightly more distorted than those present in the rutile phase of TiO_2.
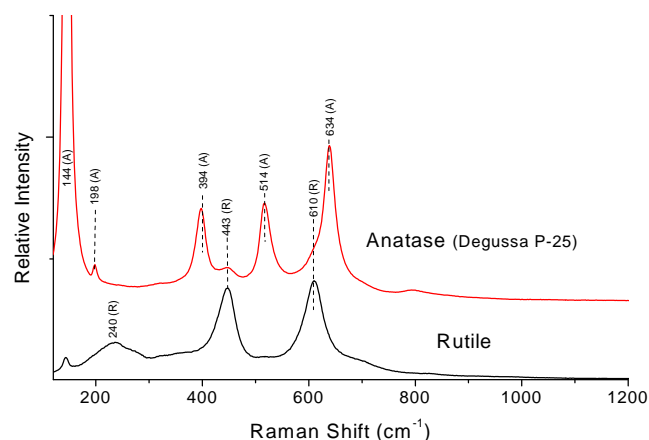

Figure 1. Raman spectra of TiO_2 bulk reference compounds: anatase (Degussa P-25) and rutile.

The Raman spectra for the Ti foil samples that were anodized to produce TiO_2 nanotubular arrays are presented in Figures 2 and 3 as a function of O_2-annealing temperature. The sample dried at room temperature, Figure 2, shows broad peaks near 612 and 467 cm^{-1} due to amorphous titania. Using length / frequency / valence relationships for titanium-oxygen bonds, Eq. (1), these broad bands are found to be consistent with TiO_6^{8-} octahedra having the same average structure as those present in both anatase and rutile phases of TiO_2 with average calculated bond lengths of *5x* 1.93 and 2.12 Å.
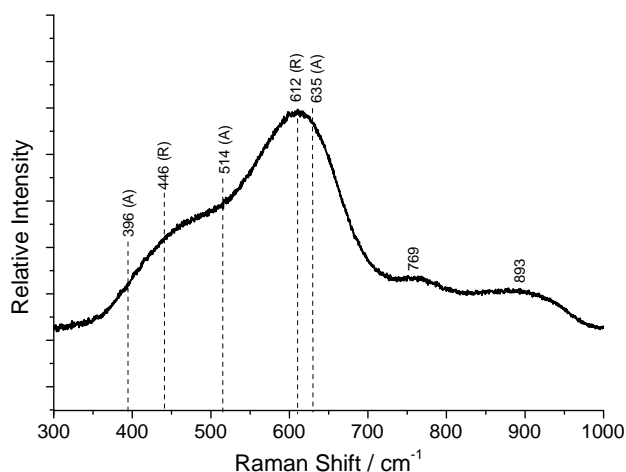
Raman Spectroscopy of Titania (TiO₂) Nanotubular Water-Splitting Catalysts

Figure 2. Raman spectra of TiO₂ nanotubes after room-temperature drying.

In addition to TiO₂ phases, Raman spectroscopy is also used to detect and identify carbon species. For the untreated TiO₂ films, amorphous carbon is present in all the films as indicated by the characteristic bands near 1342 and 1601 cm^{-1} assigned to sp^3- and sp^2-hybridized carbon, respectively (Dennison 1996); these bands are similar to those observed for carbon black. Amorphous carbonate, CO_3^{2-}, is also present in all untreated TiO₂ films as indicated by the broad but characteristic peak near 1100 cm^{-1}.
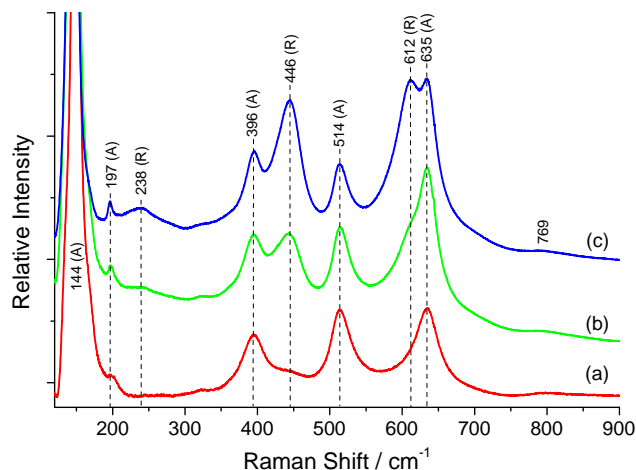

Figure 3. Raman spectra of TiO₂ nanotubular arrays after O₂-annealing at (a) 400°C, (b) 500°C, and (c) 600°C.

Annealing in oxygen at 400 °C for 6 h, Figure 3(a), results in the formation of anatase as the dominant phase in addition to a small amount of rutile. Anatase exhibits Raman bands at 635, 514, 396, and 197 cm^{-1}, as well as a very sharp and intense peak at 144 cm^{-1}.

Based on the space group D$_{4h}$[19] for anatase and assumed site symmetries for the Ti and O atoms within the unit cell (D$_{2d}$ for Ti; C$_{2v}$ for O), group-theoretical analysis shows six Raman-active "lattice vibrations" assigned as follows: A$_{1g}$ (517 cm^{-1}) + B$_{1g}$ (640 cm^{-1}) + B$_{1g}$ (397 cm^{-1}) + E$_g$ (640 cm^{-1}) + E$_g$ (147 cm^{-1}) + E$_g$ (197 cm^{-1}) (Balachandran 1982); the weak band at 796 cm^{-1} was assigned as the first overtone of the B$_{1g}$ mode. The reported crystallographic Ti-O bond lengths for bulk anatase are *4x* 1.9338 Å and *2x* 1.9797 Å (Horn 1972). Covalence / length / frequency relations show that the observed Raman bands at 640, 517, and 397 cm^{-1} are consistent with the moderately distorted TiO_6^{8-} octahedron in anatase (calculated Ti-O bond lengths: *2x* 1.89, *3x* 2.02 and 2.14 Å). The O-O covalent interactions are calculated near 246-351 cm^{-1}. The sharp peaks at 197 and 144 cm^{-1} are consistent with Ti-Ti bonding present in the octahedral chains with reported Ti-Ti bond length 2.96 Å (calculated: 2.89 and 2.96 Å, respectively). As the oxygen annealing temperature is increased from 400 to 600 °C, Figure 3(a-c), the relative amount of rutile increases as evidenced by the relative intensity increase of the Raman bands at 612, 446, and 238 cm^{-1}. For the anodized sample O₂-annealed at 600 °C, Figure 3(c), both anatase and rutile are present, with rutile being the dominant phase.

The ratio of the integrated Raman peak intensity of rutile at 446 cm^{-1} to that of anatase at 396 cm^{-1} may be used as a semi-quantitative measure of the weight ratio of rutile to anatase. The results of a recent Raman study (Zhang 2006) investigating physical mixtures of crystalline anatase and rutile revealed the following approximate and linear relationship for the weight ratio of rutile to anatase: $W_{R/A} = 3.64 \times (I_{446}/I_{396})$. We utilize this relationship in the present study of TiO₂ nanotubular films, but with the reservation that this relationship is at best semi-quantitative because the Raman scattering cross-sections of anatase and rutile change as the degree of crystallinity changes.

The Raman data and curve fitting show that the room-temperature dried film shows amorphous TiO₂, carbonate (CO_3^{2-}), and decomposition products of the ethylene-glycol electrolyte. The amorphous phase is converted to a mixture of about 3 times as much anatase as rutile 400 °C ($W_{R/A} = 0.4$), but the relative concentration of rutile increases as the O₂-annealing temperature is increased to 500 °C, where about 5 times more rutile is present ($W_{R/A} = 5$), and at 600 °C, where about 11 times more rutile is present than anatase ($W_{R/A} = 11$). The photocurrent density increases from 20 µA cm^{-2} for the dried amorphous

film to 379 μA cm^{-2} for the samples O$_2$-annealed at 500 ^{o}C, where highly crystalline rutile is the dominant phase. It has been suggested that upon annealing, the increased crystallinity results in enhanced charge transfer and photocatalytic activity (Porter 1999). O$_2$-annealing at 600 ^{o}C, however, results in a decreased photocurrent density of 349 μA cm^{-2} in spite of the increased rutile content and crystallinity in the TiO$_2$ nanotubular film.

Figure 4 shows a plot of the ratio of the integrated Raman peaks, I$_{446}$/I$_{396}$, as a function of measured photocurrent density (shown as squares, axis on the left) for the anodized TiO$_2$ films. Also shown is the measured photocurrent density as a function of O$_2$-annealing temperature (circles, axis on the right). For TiO$_2$ nanotubular films dried at room temperature, only baseline photocurrent densities of 20 μA cm^{-2} were observed for the amorphous TiO$_2$ film (not shown on the graph). After O$_2$-annealing at 400 ^{o}C, the photocurrent density increased to 58 μA cm^{-2} with the appearance of mostly crystalline anatase (72 % anatase; W$_{R/A}$ = 0.4). At 500 ^{o}C, the nanotubular film is predominantly rutile (83% rutile; W$_{R/A}$ = 5), and the photocurrent density increases significantly to 379 μA cm^{-2}, which represents the highest photocurrent density observed in this study. O$_2$-annealing at 600 ^{o}C, however, was detrimental to the PEC activity as the photocurrent density decreased slightly to 349 μA cm^{-2} where ~8% of the TiO$_2$ is anatase (W$_{R/A}$ = 11).
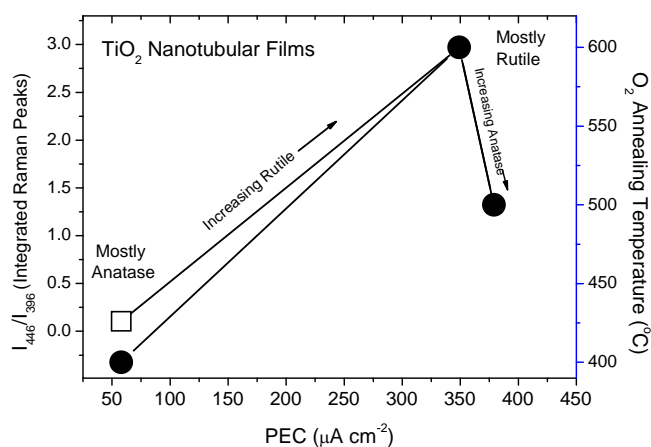

Figure 4. Plot for anodized TiO$_2$ films showing the photocurrent density (PEC) versus TiO$_2$-rutile / TiO$_2$-anatase relative concentration and O$_2$-annealing temperature. The circles correspond to the annealing temperature axis (right), and the squares correspond to the ratio of integrated Raman peaks (scale on left).

Figure 5 shows a schematic diagram of Raman-identified phases in untreated and TiO$_2$ nanotubular films as a function of O$_2$-annealing temperature and measured photocurrent density (PEC measurements: Hardcastle 2011). The anatase-to-rutile transformation occurs at much lower temperatures (~400 ^{o}C) compared to those reported for bulk samples. Previous Raman spectroscopy and X-ray diffraction studies show that the anatase-to-rutile transformation for bulk TiO$_2$ powders starts at 500 ^{o}C and is completed at about 700 ^{o}C; and for single-crystal anatase, this transformation does not occur until 900 ^{o}C (Shannon 1964).
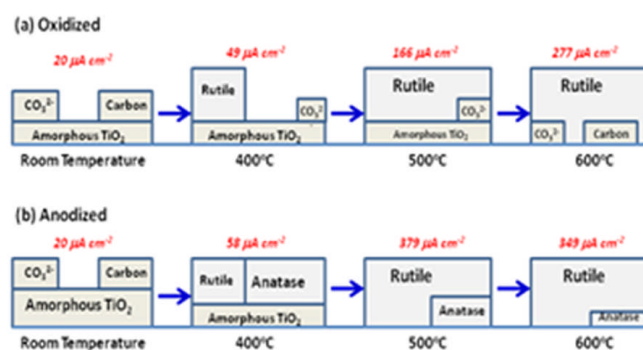

Figure 5. Scheme showing Raman-identified phases in (a) oxidized and (b) anodized films as a function of O$_2$-annealing temperature and measured photocurrent density (PEC measurements from Hardcastle, 2011).

The kinetics of the anatase-to-rutile transformation depends on many variables, including the nature and amount of Ti impurity interstitials in the TiO$_2$ lattice in addition to oxygen vacancies. These impurity ions, in this case being titanium cations having a valence less than that of Ti^{4+}, locally increase the number of oxygen vacancies in order to maintain charge neutrality. The oxygen vacancies facilitate cleavage of the Ti-O bonds in the anatase structure, which reduces the lattice volume and results in the formation of the denser rutile phase at lower annealing temperatures.

Whereas oxidized titanium foil forms only rutile, TiO$_2$ nanotubes are considerably thicker, and more "bulk-like" TiO$_2$ behavior is expected. Similar to the untreated sample, the low-crystalline rutile phase forms at 400 ^{o}C and is likely located near the oxide/metal interface, but the amorphous TiO$_2$ nanotubes located outside the oxide/metal interfacial region transform to anatase. At this temperature, about three times more anatase is present than rutile in the anodized nanotubular film. At 500 ^{o}C, there is ~5 times more rutile than anatase because the rutile formed at the

46

Raman Spectroscopy of Titania (TiO₂) Nanotubular Water-Splitting Catalysts

oxide/metal interface "seeded" or catalyzed the accelerated formation of rutile throughout the film. At 600 ^oC, the nanotubular film is mostly rutile with ~8% anatase; the anatase is presumably located at the outer edges of the film, furthest from the Ti-metal substrate. By comparison, bulk polycrystalline TiO_2 that has been O_2-annealed at 600 ^oC consists of 60% anatase.

The observed degradation of the nanotubular morphology by SEM (Hardcastle 2011) is expected with rutile formation because of the higher density and decreased surface area characteristic of the rutile phase of TiO_2. For a TiO_2 film on Ti metal, rutile formation initiates at the oxide/titanium interfacial region where oxygen vacancies are present. Collapse of the nanotubular film near the oxide/metal interfacial region is consistent with the morphological changes observed in the SEM images, where buckling of the film begins at 500 ^oC. As the annealing temperature is increased, rutile spreads out into the nanotubular layer (away from the metal surface). At 600 ^oC, where <10% anatase remains, the topical region of the nanotubular array is cracked and fragmented as the remaining anatase begins to transform to the more dense rutile phase at a temperature consistent with that of polycrystalline, unsupported anatase (500 - 700 ^oC).

We have shown using photocurrent-density measurements and Raman spectroscopy that the photoactivity of TiO_2 nanotubular arrays increases with rutile content, but reaches a maximum value at 500 ^oC, then decreases as the nanotubular morphology degrades at 600 ^oC. The increased photoactivity is attributed to the increased amount of rutile combined with the high surface area morphology. The maximun photocurrent density measured for oxidized films is 277 $\mu A\ cm^{-2}$ compared to 379 $\mu A\ cm^{-2}$ for the nanotubular films (O_2-annealed at 500 ^oC). This difference is attributed to the increase in rutile surface area provided by the TiO_2 nanotubular array architecture resulting in increased rutile photoactive sites and increased efficiency of electron transport.

Conclusions

TiO_2 is one of the most widely studied photocatalytic materials for splitting water, but the photoelectrochemical activity strongly depends on the phase composition of the material or film. The more ordered arrangement of the nanotubular TiO_2 arrays shows promise over polycrystalline TiO_2 because of observed increased efficiency of electron transport.

In this study, the photocurrent density of nanotubular TiO_2 films was correlated with the phase composition of the film as a function of oxygen annealing temperature. Raman spectroscopy was used to identify the amorphous and crystalline TiO_2 phases present in the films.

It was found that amorphous TiO_2 is converted to predominantly anatase (~72% anatase) at 400 ^oC, where the photocurrent density is comparable to that of the oxidized (untreated) film. The highest photocurrent density (2.3x that of the oxidized film) is achieved for the nanotubular film at 500 ^oC, where ~83% of the TiO_2 is rutile. At this temperature, there is enough anatase within the nanotubes to sustain its architecture and act as a support for the rutile that forms at the surface. The dramatic increase in photocurrent density is attributed to the increase in rutile surface area and corresponding photoactive sites.

At 600 ^oC, more rutile is formed (92% rutile) in the TiO_2 nanotubular film, but this is countered by the significant loss of rutile surface area due to degradation of the nanotubular array architecture. SEM images show significant degradation (from 500 to 600 ^oC) and cracking of the film as sintering occurs to accommodate the formation of the denser rutile structure. In spite of the increased rutile content, the photocurrent density decreases slightly from its value at 500 ^oC.

Literature Cited

Balachandran U and **NG Eror**. 1982. Raman spectrum of titanium dioxide. Journal of Solid State Chemistry 42:276-82.

Bendavid A, PJ Martin, A Jamting, and **H Takikawa**. 1999. Structural and optical properties of titanium oxide thin films deposited by filtered arc deposition. Thin Solid Films 355-56:6-11.

Burda C, **Y Lou**, **X Chen**, **ACS Semia**, **J Stout** and **JL Gole**. 2003. Enhanced nitrogen doping in TiO_2 nanoparticles. Nano Letters 3:1049-51.

Cromer DT and **K Herrington**. 1955. The Structures of Anatase and Rutile. Journal of the American Chemical Society. **77:** 4708-9.

Dennison JR, M Holtz and **G Swain**. 1996. Raman spectroscopy of carbon materials. Spectroscopy. 11(8):38-46.

Fujishima A and **K Honda**. 1972. Electrochemical Photolysis of Water at a Semiconductor Electrode. Nature 238:37-8.

Hardcastle FD and **IE Wachs**. 1990. Determination of molybdenum-oxygen bond distances and bond orders by Raman spectroscopy. Journal of Raman Spectroscopy 21:683-91.

Hardcastle FD and **IE Wachs**. 1991. Determination of vanadium-oxygen bond distances and bond orders by Raman spectroscopy. The Journal of Physical Chemistry 5:5031-41.

Hardcastle FD, **H Ishihara**, **R Sharma** and **AS Biris**. 2011. Photoelectroactivity and Raman spectroscopy of anodized titania photoactive water-splitting catalysts as a function of oxygen-annealing temperature. Journal of Materials Chemistry 21:6337-45.

Heald EF and **CW Weiss**. 1972. Kinetics and mechanism of the anatase/rutile transformation, as catalyzed by ferric oxide and reducing conditions. American Mineralogist 57:10-23.

Horn M, **CF Schwerdtfeger** and **EP Meagher**. 1972. Refinement of the structure of anatase at several temperatures. Zeitschrift fur Kristallographie 136:273-81.

Ishihara H, **JP Bock**, **R Sharma**, **FD Hardcastle**, **GK Kannarpady**, **MK Mazumbder** and **AS Biris**. 2010. Electrochemical synthesis of titania nanostructural arrays and their surface modification for enhanced photoelectrochemical hydrogen production. Chemical Physics Letters 489:81-5.

Liu Z, **B Pesic**, **KS Raja**, **RR Rangaraju** and **M Misra**. 2009. Hydrogen generation under sunlight by self ordered TiO_2 nanotube arrays. International Journal of Hydrogen Energy 34:3250-7.

Porter JF, **Y Li** and **CK Chan**. 1999. The effect of calcination on the microstructural characteristics and photoreactivity of Degussa P-25 TiO_2. Journal of Materials Science 34:1523-31.

Shannon RD and **JA Pask**. 1964. Topotaxy in the anatase-rutile transformation. The American Mineralogist 49: 1707-17.

Sharma R, **PP Das**, **M Misra**, **V Mahajan**, **P Bock**, **S Trigwell**, **AS Biris** and **MK Mazumder**. 2009. Enhancement of the photoelectrochemical conversion efficiency of nanotubular TiO_2 photoanodes using nitrogen plasma assisted surface modification. Nanotechnology 20:075704.

Wang J, **L Zhao**, **VS-Y Lin** and **Z Lin**. 2009. Formation of various TiO_2 nanostructures from electrochemically anodized titanium. Journal of Materials Chemistry 19: 3682-7.

Zhang Z, **M Li**, **Z Feng**, **J Chen** and **C Li**. 2006. UV Raman spectroscopic study on TiO_2. I. Phase Transformation at the Surface and in the bulk. Journal of Physical Chemistry B. 110:927-35.

48